Probing the Interaction between Prostacyclin Synthase and Prostaglandin H-2 Analogues or Inhibitors via a Combination of Resonance Raman Spectroscopy and Molecular Dynamics Simulat...

ARTICLE *in* JOURNAL OF THE AMERICAN CHEMICAL SOCIETY · NOVEMBER 2011

Impact Factor: 12.11 · DOI: 10.1021/ja206918w · Source: PubMed

JACS
JOURNAL OF THE AMERICAN CHEMICAL SOCIETY

ARTICLE

pubs.acs.org/JACS

Probing the Interaction between Prostacyclin Synthase and Prostaglandin H_2 Analogues or Inhibitors via a Combination of Resonance Raman Spectroscopy and Molecular Dynamics Simulation Approaches

Wei-Chih Chao,[†] Jyh-Feng Lu,[‡] Jinn-Shyan Wang,[*,‡] Hsiao-Ching Yang,[*,§] Hsiao-Hui Chen,[§] Yi-Kang Lan,[§] Ya-Chien Yu,[∥] Pi-Tai Chou,[*,∥] and Lee-Ho Wang[⊥]

[†]Graduate Institute of Applied Science and Engineering, [‡]School of Medicine, and [§]Department of Chemistry, Fu-Jen Catholic University, New Taipei City 24205, Taiwan, Republic of China

[∥]Department of Chemistry, National Taiwan University, Taipei, Taiwan, Republic of China

[⊥]Division of Hematology, Department of Internal Medicine, University of Texas Health Science Center, Houston, Texas, United States

Supporting Information

ABSTRACT: In an aim to probe the structure−function relationship of prostacyclin synthase (PGIS), resonance Raman (RR) spectroscopy and molecular dynamic (MD) simulation approaches have been exploited to characterize the heme conformation and heme−protein matrix interactions for human PGIS (hPGIS) and zebrafish PGIS (zPGIS) in the presence and absence of ligands. The high-frequency RR (1300−1700 cm^{-1}) indicates that the heme group is in the ferric, six-coordinate, low-spin state for both resting and ligand-bound hPGIS/zPGIS. The low-frequency RR (300−500 cm^{-1}) and MD simulation reveal a salient difference in propionate−protein matrix interactions between hPGIS and zPGIS, as evident by a predominant propionate bending vibration at 386 cm^{-1} in resting hPGIS, but two vibrations near 370 and 387 cm^{-1} in resting zPGIS. Upon binding of a substrate analogue (U46619, U51605, or U44069), both hPGIS and zPGIS induce a distinctive perturbation of the propionate−protein matrix interactions, resulting in similar Raman shifts to ∼381 cm^{-1}. On the contrary, the bending vibration remains unchanged upon binding of inhibitor/ligand (minoxidil, clotrimazole, or miconazole), indicating that these inhibitors/ligands do not interfere with the propionate−protein matrix interactions. These results, together with subtle changes in vinyl bending modes, demonstrate drastically different RR shifts with heme conformational changes in both hPGIS and zPGIS upon different ligand bindings, suggesting that PGIS exhibits a ligand-specific heme conformational change to accommodate the substrate binding. This substrate-induced modulation of the heme conformation may confer high product fidelity upon PGIS catalysis.

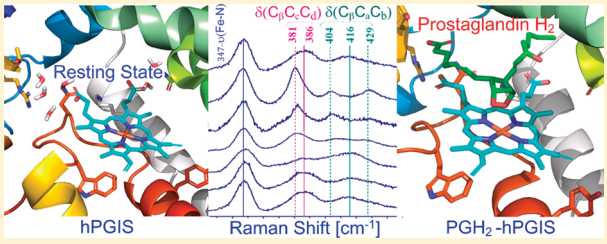

INTRODUCTION

Prostacyclin synthase (PGIS), an endoplasmic reticulum membrane protein, catalyzes an isomerization of prostaglandin H_2 (PGH_2) to form prostacyclin I_2 (PGI_2), as shown in Figure 1. PGI_2 is primarily produced in the vascular endothelium and plays an important role in the local control of vascular tone and platelet aggregation.[1] Accumulating evidence suggests that PGI_2 contributes to a variety of cardiovascular and pulmonary diseases such as thrombosis, atherosclerosis, myocardial infarction, and primary pulmonary hypertension.[2,3] PGIS was first isolated from aorta.[4] The enzyme was later purified to homogeneity as a 52 kDa hemoprotein with spectroscopic characteristics of cytochrome P450[5,6] and was assigned to the P450 superfamily on the basis of sequence homology.[7] A typical P450 monooxygenase reaction requires molecular oxygen and a reductase to transfer electrons from NAD(P)H to the heme moiety, whereas PGIS catalyzes an isomerization of an endoperoxide without the need for molecular oxygen, reductase, or any other external electron donors.[8]

UV−vis, magnetic circular dichroism (MCD), and electron paramagnetic resonance (EPR) spectra indicate that the resting PGIS has a typical low-spin ferric heme.[9] The active site of PGIS is very flexible to accommodate large and hydrophobic ligands via an induced-fit mechanism. X-ray crystallographic analyses of ligand-free PGIS demonstrate that PGIS exhibits a typical P450 triangular prism-shaped tertiary core structure, though differences in the heme peripheral structure are remarkable.[10,11] The heme moiety of PGIS is deeply buried between the I and L helices, but the heme propionate−protein scaffold interactions are largely absent, in contrast to most P450 proteins in which the extensive propionate−protein matrix interactions are commonly

Received: July 24, 2011
Published: October 06, 2011

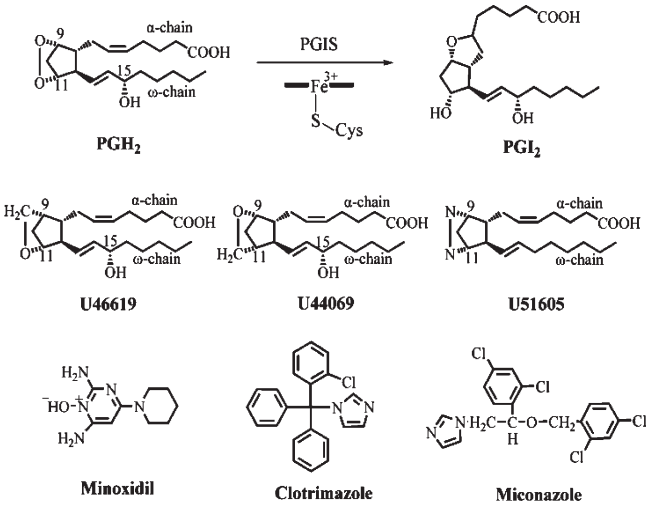

Figure 1. Structures of PGH_2, PGI_2, and various binding ligands for PGIS.

observed. The propionate and vinyl peripheral groups (Figure 2) have long been considered as key structural determinants of the heme reactivity, whose influence may be sensitively manipulated by protein−heme interactions.[12−14]

Since the reaction of PGH_2 catalyzed by PGIS, forming PGI_2 (Figure 1), is too fast to have structural resolution, structural analogues are widely used to mimic the binding of substrate into the heme pocket of PGIS. X-ray crystal structures of PGH_2 analogue U51605-bound and inhibitor minoxidil-bound PGIS have revealed a stereospecific substrate binding of PGIS and unveiled its unique features that facilitate isomerization.[11] Upon substrate analogue U51605 binding, the heme group of PGIS undergoes significant ligand-induced conformational change, leading to the recovery of the propionate−protein matrix interactions found in other P450s. In minoxidil-bound PGIS, however, the propionate−protein interactions are unable to recover. Thus, the heme propionate−protein interactions are observed only when the canonical substrate is ligated to the heme moiety of PGIS, implying that the propionate−protein interactions play an important functional role in PGIS.

While the elegant X-ray analyses provide valuable information on the structure of PGIS as well as PGIS−substrate analogue interactions in a single crystal, supplementary methods must be used to determine the structural and functional interactions that are important in solution and to examine the dynamic basis of enzyme−substrate/ligand interactions. Resonance Raman (RR) spectroscopy has long been recognized as a valuable tool for providing detailed information about the active site structure of heme proteins.[15,16] Particularly, the vibration modes in the low-frequency (300−500 cm^{-1}) region of RR spectra associated with the heme propionate and vinyl groups in the P450 family are well established[13,17,18] and can thus serve as comparative references for probing subtle structural perturbations in the heme environment.

To gain a better understanding of the structure/function of PGIS, we herein employ RR spectroscopy to examine subtle changes in the structure of the heme and heme environment of PGIS upon the binding of PGH_2 analogues U46619, U51605, and U44069 as well as three known PGIS inhibitors/ligands, minoxidil, clotrimazole, and miconazole (Figure 1). PGH_2 analogues U46619, U51605, and U44069 have been used

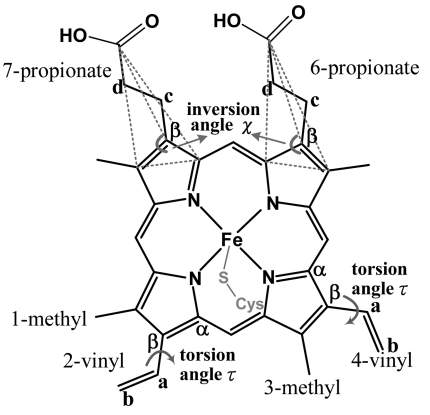

Figure 2. Structures of the heme groups of PGIS.

previously by Ullrich and co-workers to unveil the catalytic mechanism of PGIS and its counterpart enzyme thromboxane synthase (TXAS).[8,19] Minoxidil is reported to be a potent PGIS inhibitor,[20] whereas miconazole is an inhibitor for TXAS.[21] Clotrimazole is a bulky ligand, which binds PGIS with high affinity and has been used for spectroscopic probing of the heme active site in PGIS.[9] We also took molecular dynamics (MD) simulation approaches to rationalize the experimental results and to gain in-depth insight into the heme−protein interactions. We further compared the RR spectra and computational data for human PGIS (hPGIS) and zebrafish PGIS (zPGIS) to explore the subtle changes in heme microenvironments upon ligand binding. A recent study has shown that hPGIS and zPGIS exhibit nearly identical three-dimensional structures and enzymatic activity, though they share only 45% sequence identity.[11] Our results provide evidence that although the structures of heme and its environment are different between hPGIS and zPGIS, they converge to the same structure upon substrate binding.

MATERIALS AND METHODS

Materials. Substrate analogues U51605 (9,11-azoprosta-5,13-dienoic acid), U46619 [15-hydroxy-9,11-(methanoepoxy)prosta-5,13-dienoic acid], and U44069 [15-hydroxy-9,11-(epoxymethano)prosta-5,13-dienoic acid] were purchased from Cayman. Inhibitors/ligands minoxidil [6-(1-piperidyl)-2,4-diaminopyrimidine 3-oxide], clotrimazole [1-(*o*-chloro-α,α-diphenylbenzyl)imidazole], and miconazole [1-[2,4-dichloro-β-[(2,4-dichlorobenzyl)oxy]phenyl]imidazole] were acquired from Sigma-Aldrich.

Purification of Recombinant hPGIS and zPGIS. Recombinant hPGIS and zPGIS were expressed and purified as described previously.[9,11] In brief, the constructs were designed by replacing the first 17 and 16 amino acid residues in the N-terminal transmembrane domain with a hydrophilic sequence, MAKKTSS, for human and zebrafish cDNA, respectively. A four-histidine tag was added to the C-terminus of both constructs for facilitating protein purification. The resulting PGIS cDNAs were transformed into *Escherichia coli* strain BL21/(DE3)pLys for protein expression. The recombinant PGIS was purified to electrophoretic homogeneity by Ni−NTA (Qiagen) and CM (carboxymethyl) Sepharose chromatography. The concentration of the enzyme was determined on the basis of $\varepsilon_{418\ nm}$= 100 mM^{-1} cm^{-1} and was adjusted to 40 μM by 20 mM KPi, pH 7.2, containing 10% glycerol before use.

Resonance Raman Spectroscopy. RR spectra were collected by a triple-stage spectrograph (PI acton TriVista TR555) coupled with a liquid nitrogen cooled CCD detector (Spec10:100BR/LN). The system

dx.doi.org/10.1021/ja206918w |*J. Am. Chem. Soc.* 2011, 133, 18870–18879

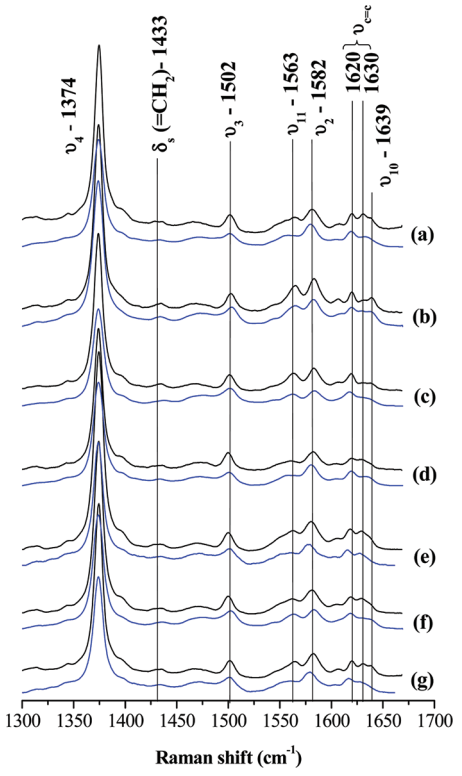

Figure 3. High-frequency RR spectra of various forms of 40 μM hPGIS (black line) and zPGIS (blue line) excited at 413.1 nm: (a) resting, (b) with 150 μM U46619, (c) with 150 μM U51605, (d) with 285 μM U44069, (e) with 150 μM minoxidil, (f) with 150 μM clotrimazole, and (g) with 150 μM miconazole.

is operated under an additive mode to achieve a spectral resolution of ~1.0 cm^{-1} (at 500 nm). The gratings with 1800 g/mm were used on each stage. The 413.1 nm line (~20 mW) from a krypton ion laser (Spectra-Physics Beamlok 2060) was used as the excitation wavelength, which was focused onto the sample in a 135° backscattering geometry. The Raman shifts were calibrated by the use of cyclohexane solvent as a standard. Spectral manipulation such as baseline correction/adjustment and band component analysis was performed using the PeakFit v4.02 software package. Band fitting was carried out for the low-frequency RR spectra using a Gauss−Lorentz cross-product function. The minimum number of components used for the fitting process is based on the reported bending modes relevant to the propionate and vinyl bending conformers. The fitting allows the Lorentz:Gauss ratio (0.0 = pure Gauss, 1.0 = pure Lorentz) to vary, and deconvolution was undertaken until reproducible results were obtained with a squared regression coefficient R^2 around 0.99. Spectral deconvolution was done as well with the Lorentz:Gauss ratio fixed at a value of 0.5. This then allows a comparison of the deconvolution spectra fitted with a variable line shape and those using a fixed Lorentz−Gauss fitting; we have added detailed information about line shapes (shape, position, and width) and R^2 to the Supporting Information (Tables S1 and S2).

MD Simulations of Substrate/Analogue-Bound hPGIS. The initial structure of hPGIS was taken from the Protein Data Bank (PDB entry code 2IAG). The structures of substrate PGH_2 and analogues U46619, U44069, and U51605 were constructed by geometry optimization with CHARMM force field calculation. We took into account the flexibility of the substrate analogue side chains by generating conformations using the systematic search algorithm of the Cerius^2 software.[22,23] Docking experiments were carried out using the CHARMM-based molecular dynamics docking algorithm implemented in the program.[22−24] The grid maps for atoms involved were generated for an approximate radius of 13.0 Å of a sphere centered above the heme iron. Each PGH_2 analogue conformation was geometrically docked to the hPGIS active site, taking into account both the shape complementarity and docking energy. The analogue flexibility was addressed by including different orientations of its rotatable side chains in the docking procedure. Accordingly, 10^8 conformation structures were generated, among which, following the statistics, representatives of 400 stable conformations were obtained for analysis of the PGH_2 analogue-bound PGIS complex. The remaining results were minimized, and the lowest energy docking result was used as a starting point for further MD simulations. Details of the computational approach are given in the Supporting Information.

RESULTS

High-Frequency RR Spectra of Resting and Ligand-Bound PGIS. The high-frequency (1300−1700 cm^{-1}) RR spectra of all hPGIS and zPGIS complexes obtained using the 413.1 nm krypton laser line are shown in Figure 3; pertinent data are summarized in Table 1. The high-frequency region contains the porphyrin skeletal stretching bands that are known to be sensitive to the oxidation state, core size, and spin state of the heme group.[25−27] Both resting hPGIS and resting zPGIS exhibit characteristic vibration frequencies at 1374, 1502, 1582, 1639, and 1433 cm^{-1} that are assignable to the porphyrin skeletal modes υ_4, υ_3, υ_2, υ_{10}, and $\delta_s(=CH_2)$, respectively (Table 1). These bands are characteristic for six-coordinate, low-spin ferric heme species. Two vinyl stretching vibrations ($\upsilon_{C=C}$) at about 1620 and 1630 cm^{-1} can be assigned to in-plane and out-of-plane vinyl conformers, respectively.[28] The observations indicate that resting hPGIS and zPGIS have similar heme structures in terms of the oxidation state, core size, and spin state.

RR spectra were also obtained for hPGIS and zPGIS complexed with substrate analogues or inhibitors. U46619 (O-based ligand) and U51605 (N-based ligand) are two known stable analogues of PGH_2, which bind to PGIS with K_d values of 36 and 1.9 μM, respectively.[9,11] U44069, a C-9 carbon replacing an oxygen atom of PGH_2, has weak affinity for PGIS with a K_d > 190 μM on the basis of the absorption spectral perturbation method.[8,9] As for the inhibitor, minoxidil has long been thought to be a N-based ligand with a K_d of ~5 μM,[20] but a recent X-ray structure revealed that the oxygen of minoxidil is ligated to the heme iron.[11] Clotrimazole, a bulky and rigid imidazole derivative, binds tightly to PGIS with a K_d of 0.94 μM.[9] Miconazole, bulky but more flexible than clotrimazole, binds to PGIS with a K_d of 1.89 μM.[32] Table 1 shows that the υ_4, υ_3, υ_2, and υ_{10} vibrations of the complexes are very similar to those of resting hPGIS and zPGIS, all being characteristic of a low-spin six-coordinated state, as is typical for substrate-free P450s.[12,14−16,33] The frequencies of two vinyl stretching vibrations of these complexes are also similar to those of resting hPGIS and zPGIS, though the relative intensities of bands at about 1620 and 1630 cm^{-1} vary slightly among the complexes, as presented in the detailed deconvoluted spectra in Figure S1 of the Supporting Information.

Low-Frequency RR Spectra of Resting and Ligand-Bound PGIS. RR studies of various heme-containing P450 enzymes have revealed that the low-frequency vibration modes around 300−500 cm^{-1} are sensitive to the heme environmental changes. Parts A and B of Figure 4 show the low-frequency RR spectra of resting PGH_2 analogue- and inhibitor/ligand-bound hPGIS and zPGIS. The spectral patterns exhibit the modes associated with the heme skeletal vibration (υ_8, $\upsilon(Fe-N_{pyr})$ stretching),

Table 1. Assignments of the High-Frequency Resonance Raman Bands of PGIS and Comparison with Other P450 Heme Proteins

protein	υ_4 (cm^{-1})	$\delta_s(=CH_2)$ (cm^{-1})	υ_3 (cm^{-1})	υ_2 (cm^{-1})	υ_{10} (cm^{-1})	heme structure	ref
hPGIS	1374	1433	1502	1582	1639	6C/LS	this paper
hPGIS−U46619	1374	1434	1502	1583	1639	6C/LS	this paper
hPGIS−U51605	1374	1434	1502	1583	1638	6C/LS	this paper
hPGIS−U44069	1374	1434	1502	1583	1638	6C/LS	this paper
hPGIS−minoxidil	1374	1433	1502	1582	1638	6C/LS	this paper
hPGIS−clotrimazole	1374	1433	1502	1582	1638	6C/LS	this paper
hPGIS−miconazole	1374	1433	1502	1582	1638	6C/LS	this paper
zPGIS	1374	1434	1502	1582	1638	6C/LS	this paper
zPGIS−U46619	1374	1434	1502	1583	1638	6C/LS	this paper
zPGIS−U51605	1374	1434	1502	1582	1638	6C/LS	this paper
zPGIS−U44069	1374	1434	1502	1582	1638	6C/LS	this paper
zPGIS−minoxidil	1374	1434	1502	1582	1638	6C/LS	this paper
zPGIS−clotrimazole	1374	1434	1502	1582	1638	6C/LS	this paper
zPGIS−miconazole	1374	1434	1502	1582	1639	6C/LS	this paper
TXAS	1374		1503	1587	1638	6C/LS	13
P450	1373		1503	1584	1635	6C/LS	29
P450 BM3	1373.8		1502.1	1582.8	1637.7	6C/LS	14
P450 BM3-AA	1371.9		1486.6	1569.5		5C/HS	14
eNOS	1374		1503	1579	1638	6C/LS	30
CYP3A4	1373		1502	1586	1643	6C/LS	31

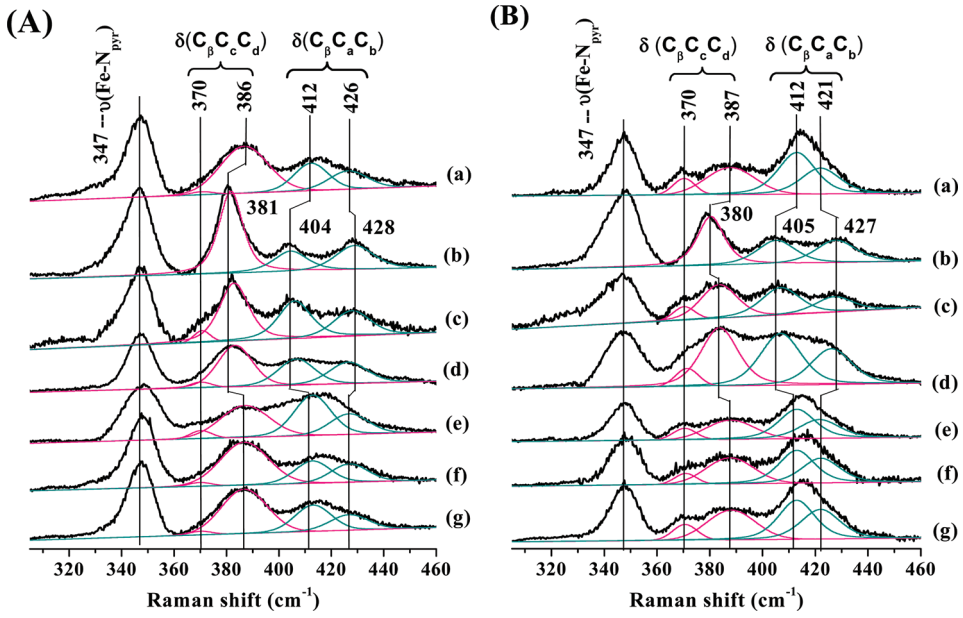

Figure 4. Low-frequency RR spectra of various forms of 40 μM (A) hPGIS and (B) zPGIS excited at 413.1 nm: (a) resting, (b) with 150 μM U46619, (c) with 150 μM U51605, (d) with 285 μM U44069, (e) with 150 μM minoxidil, (f) with 150 μM clotrimazole, and (g) with 150 μM miconazole. Spectra were deconvoluted as described in the text. Key: black solid curves, experimental data; red curves, modes associated with $\delta(C_\beta C_c C_d)$ propionate bending; dark cyan curves, modes associated with $\delta(C_\beta C_a C_b)$ vinyl bending.

"propionate bending" region ($\delta(C_\beta C_c C_d)$), and "vinyl bending" modes ($\delta(C_\beta C_a C_b)$) (see Figure 2 for the definitions); the nomenclature in quotations is in accordance with the reported studies.[12−14,33] The heme skeletal vibration near 347 cm^{-1} (υ_8, $\upsilon(Fe-N_{pyr})$ stretching)[33] is unaffected by the binding of either substrate analogues or inhibitors. However, the $\delta(C_\beta C_c C_d)$ and $\delta(C_\beta C_a C_b)$ bending modes are remarkably perturbed by a substrate analogue (U46619, U51605, or U44069) and an inhibitor/ligand (minoxidil, clotrimazole, or miconazole) (Figure 4, black curves). Furthermore, the spectral patterns perturbed by a substrate analogue and an inhibitor/ligand appear to be different. To evaluate these spectral patterns, the low-frequency spectra were deconvoluted, and the resulting modes associated with propionate and vinyl bending are shown in red and dark cyan curves, respectively (Figure 4). The peak center frequencies, bandwidths, and relative integrated intensities among peaks (as indicated in parentheses) resulting from deconvolution analyses are tabulated in Table 2, and detailed information regarding the bandwidth,

Table 2. Assignments of the Low-Frequency Resonance Raman Bands of PGIS and Comparison with Other Heme Proteins

protein	ν_8 (cm^{-1})	$\delta(=C_\beta C_c C_d)$ (cm^{-1}) (bwth[a], integ,[b] %)	$\delta(=C_\beta C_a C_b)$ (cm^{-1}) (bwth[a], integ,[b] %)	ref
hPGIS	347	370 (10, 3), 386 (22, 97)	412 (15, 57), 426 (17, 43)	this paper
hPGIS−U46619	347	381 (11, 100)	404 (15, 45), 428 (17, 55)	this paper
hPGIS−U51605	347	370 (8, 8), 382 (13, 92)	405 (15, 59), 427 (17, 41)	this paper
hPGIS−U44069	347	370 (9, 7), 383 (15, 93)	406 (16, 53), 426 (17, 47)	this paper
hPGIS−minoxidil	347	370 (9, 9), 386 (22, 91)	412 (16, 66), 426 (17, 34)	this paper
hPGIS−clotrimazole	347	370 (10, 4), 386 (22, 96)	412 (16, 55), 426 (17, 45)	this paper
hPGIS−miconazole	347	370 (10, 4), 386 (21, 96)	412 (16, 61), 426 (17, 39)	this paper
zPGIS	347	370 (10, 21), 387 (22, 79)	412 (17, 61), 421 (18, 39)	this paper
zPGIS−U46619	347	380 (12, 100)	405 (17, 50), 427 (18, 50)	this paper
zPGIS−U51605	347	370 (10, 18), 383 (16, 82)	406 (17, 64), 427 (17, 36)	this paper
zPGIS−U44069	347	371 (10, 14), 383 (17, 86)	406 (18, 59), 426 (18, 41)	this paper
zPGIS−minoxidil	347	370 (10, 22), 387 (21, 78)	412 (16, 59), 421 (18, 41)	this paper
zPGIS−clotrimazole	347	370 (10, 16), 387 (21, 84)	412 (16, 56), 422 (17, 44)	this paper
zPGIS−miconazole	347	370 (11, 21), 387 (21, 79)	412 (16, 55), 421 (18, 45)	this paper
TXAS	340	378	408, 424	13
TXAS−U44069	343	368, 378	410, 425	13
TXAS−U46619	342	368, 378	409, 424	13
TXAS−miconazole	344	369, 379	410, 424	13
P450	347	379	424	29
P450 BM3	344	380	393, 422	14
P450 BM3-AA	344	366, 380	405, 416, 428	14
metMb	344	376	409, 440	33
deoxy Mb	342	370	405, 436	33
CPY3A4	344	370, 378	411, 423	31

[a] Bandwidth. [b] Relative integrated intensity (%).

Lorentz:Gauss ratio, and squared regression coefficient is given in Table S1 of the Supporting Information.

For the propionate bending mode $\delta(C_\beta C_c C_d)$ of the resting hPGIS (Figure 4A, trace a), the broad peak at 386 cm^{-1} is fit best with one Gaussian band and a minor shoulder band at 370 cm^{-1}, yielding an integrated population ratio of 97:3 shown in Table 2. This assignment is supported by the observation of the propionate conformers associated with the heme peripheral group dispositions.[12,14,33] Figure 4A also reveals that the inhibitor/ligand-perturbed propionate bending mode (traces e−g) exhibits no significant Raman shifts from resting hPGIS (trace a). In sharp contrast, binding of substrate analogues (traces b−d) induces the propionate bending mode to shift substantially to a lower frequency near 381 cm^{-1}. Similar to hPGIS, zPGIS exhibits inhibitor/ligand-perturbed RR spectra (Figure 4B, traces e−g) essentially identical to that of the resting form (trace a), which has two vibrations near 370 and 387 cm^{-1}. However, binding of substrate analogues (traces b−d) induces a substantial change of the propionate bending mode that shifts to 380 cm^{-1}.

Deconvolution analyses of the vinyl bending mode $\delta(C_\beta C_a C_b)$ in the region of ∼400−430 cm^{-1} fit the broad peak into two peaks (parts A and B of Figure 4, trace a), yielding a higher intensity mode at 412 cm^{-1} and a lower intensity mode at 426 cm^{-1} for resting hPGIS (412 and 421 cm^{-1} for resting zPGIS). The integrated intensity ratios are shown in Table 2. These two modes were expected to be associated with in-plane and out-of-plane distortions of the heme macrocycle, which are activated by altering the orientation of the heme peripheral substituents.[12,14,33,34] Notably, substrate analogue binding has an influence on the disposition of the vinyl bending mode, as evidenced by the split to 404 and 428 cm^{-1} for hPGIS (405 and 427 cm^{-1} for zPGIS).

In stark contrast to other analogue-bound PGISs, the U46619-bound hPGIS reveals remarkably different behavior in propionate bending modes, which possesses an intense 381 (380 in zPGIS) cm^{-1} peak with a narrower bandwidth and exhibits a relatively higher Lorentz:Gauss ratio (see Table S1 of the Supporting Information). Notably, the distinctive 370 cm^{-1} band in zPGIS disappears upon U46619 binding. As shown in Table S1, the deconvoluted spectral analyses reveal that binding of U46619 causes not only changes of the RR signals but also a higher Lorentz:Gauss ratio for either the propionate bending peaks or the vinyl bending, as compared to that of other analogues or inhibitors. Also, the deconvoluted spectra of inhibitor-bound PGIS reveal no significant differences from that of the resting form. The results indicate that substrate analogue binding influences the disposition of the propionate and vinyl motions. Differences between resting and ligand-bound PGIS suggest the variability in heme-peripheral flexibility, which may play an important role in enzyme catalysis.

Molecular Structure Analyses. The RR data prompted us to carry out MD simulations to gain insight into the structures of substrate/analogue (PGH_2/U51605, U46619, and U44069) bound hPGIS/zPGIS. Except for U51605-bound zPGIS, all structures remain unsolved to date. These simulated structures provide a structural basis not only for unresolved structures but also for a comparison with the resolved crystal structures.[11] Pertinent data are summarized in Tables 3 and 4 (also, see the Supporting Information). Both zPGIS[11] and hPGIS[10] in the resting state contain at least 10 tightly bound water molecules at

Table 3. Comparison of the Ligand-Free and U51605-Bound hPGIS and zPGIS Structures

	distance (Å)			distance (Å)	
ligand environment	hPGIS[a]	U51605+hPGIS[b]	ligand environment	zPGIS[c]	U51605+zPGIS[c]
Fe−C_9N		3.03	Fe−C_9N		3.12
Fe−C_{11}N		2.60	Fe−C_{11}N		2.29
N287−C_9N		2.80	N277−C_9N		2.25
N287−C_{11}N		3.05	N277−C_{11}N		3.42
T358−COOH(U)		4.28	T338−COOH(U)		1.59
R359−COOH(U)		4.52	R339−COOH(U)		2.64
N439−COOH(U)		1.96	N419−COOH(U)		3.61
	distance (Å)			distance (Å)	
heme environment	hPGIS[a]	U51605+hPGIS[b]	heme environment	zPGIS[c]	U51605+zPGIS[c]
Fe−S	2.53	2.39	Fe−S	2.35	2.29
6-propionate with K121	3.69	1.91	6-propionate with K119	2.32	3.53
6-propionate with Q280	2.44	4.87	6-propionate with Q270	6.83	9.33
6-propionate with N439	5.67	5.37	6-propionate with N419	6.72	2.43
6-propionate with wat212	1.75		6-propionate with Q94	5.36	1.92
7-propionate with COOH(U)		1.96	7-propionate with COOH(U)		1.82
7-propionate with F96	7.20	8.15	7-propionate with Q94	3.56	2.11
7-propionate with R359	6.31	4.04	7-propionate with R339	4.57	1.78
7-propionate with N439	3.62	2.79	7-propionate with N419	5.7	2.53
7-propionate with wat207	2.18		7-propionate with wat63	1.94	
7-propionate with wat211	3.90	1.95	7-propionate with wat149	3.08	
7-propionate with wat208	3.64		7-propionate with wat122	3.52	2.37
7-propionate with wat209	4.32		7-propionate with wat42	2.00	
2-vinyl−W434	3.84	3.65	2-vinyl−W414	3.73	3.88
4-vinyl−Y446	3.23	3.66	4-vinyl−F126	3.75	3.79

[a] The structure of resting hPGIS was taken from the Protein Data Bank (PDB entry code 2IAG). [b] MD simulation structure of U51605-bound hPGIS. [c] The crystal structures of resting zPGIS and U51605-bound zPGIS were taken from PDB entry codes 3B98 and 3B99.

Table 4. Comparison of the Heme Propionate and Vinyl Motions for Ligand-Free and U51605-Bound hPGIS and zPGIS Structures

	χ(out of plane) (deg)			χ(out of plane) (deg)	
propionate inversion angle[a]	hPGIS	U51605+hPGIS	propionate inversion angle[a]	zPGIS	U51605+zPGIS
6-propionate	56	−7	6-propionate	31	−18
7-propionate	26	19	7-propionate	20	22
	$\tau(C_\alpha C_\beta C_a C_b)$ (deg)			$\tau(C_\alpha C_\beta C_a C_b)$ (deg)	
vinyl torsion[b]	hPGIS	U51605+hPGIS	vinyl torsion[b]	zPGIS	U51605+zPGIS
2-vinyl	−150 to −137	−166 to −150	2-vinyl	−162	178
4-vinyl	153 to 66	147 to 74	4-vinyl	160	−140

[a] Propionate inversion angle χ defined in Figure 2. A positive χ value means propionate is raised in the heme distal pocket, whereas a negative χ value means propionate lies on the heme proximal side. [b] Vinyl torsion $\tau(C_\alpha C_\beta C_a C_b)$ defined in Figure 2. Values closer to ±180° correspond to vinyl restriction to the in-plane conformation; otherwise the detergency from 180° corresponds to a more flexible vinyl with an out-of-plane conformation.

the active site. Only those water molecules involved in the hydrogen-bonding networks with propionate groups are shown in Figure 5, while water molecules on the distal side of heme are intentionally ignored. Notably, the microenvironments around heme are different between the resting hPGIS and resting zPGIS. 7-Propionate in the resting zPGIS forms extended hydrogen-bonding networks via water molecules to the residues R339 and N419 (Figure 5B). In contrast, 7-propionate of the resting hPGIS is hydrogen-bonded to a distinct cluster of water molecules (Figure 5A). On the other hand, 6-propionate in hPGIS forms hydrogen bonds to Q280 and a water network (Figure 5A), whereas 6-propionate in zPGIS binds tightly and solely to K119 (Figure 5B).

Figure 6A depicts a consensus mode of U51605−hPGIS complex formation based on the MD trajectory analysis. The

dx.doi.org/10.1021/ja206918w |J. Am. Chem. Soc. 2011, 133, 18870–18879

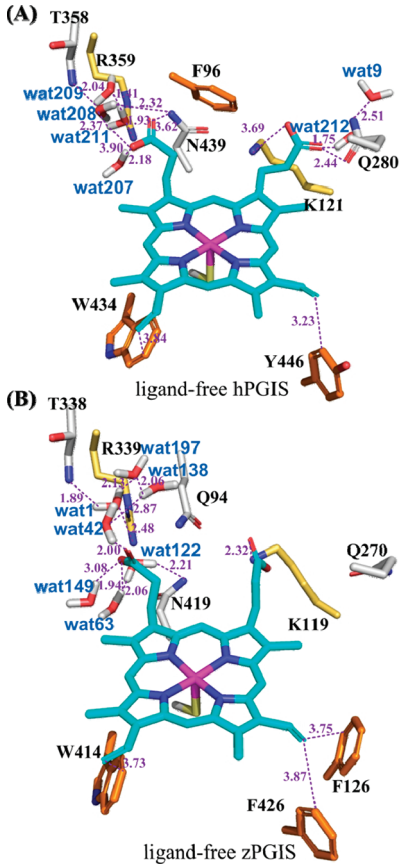

Figure 5. Molecular structure analyses for the resting state of (A) hPGIS and (B) zPGIS. The heme is shown as sticks with nitrogen atoms in blue and oxygen in red. The protein residues and water molecules involved in the hydrogen-bonding networks with propionate groups are indicated.

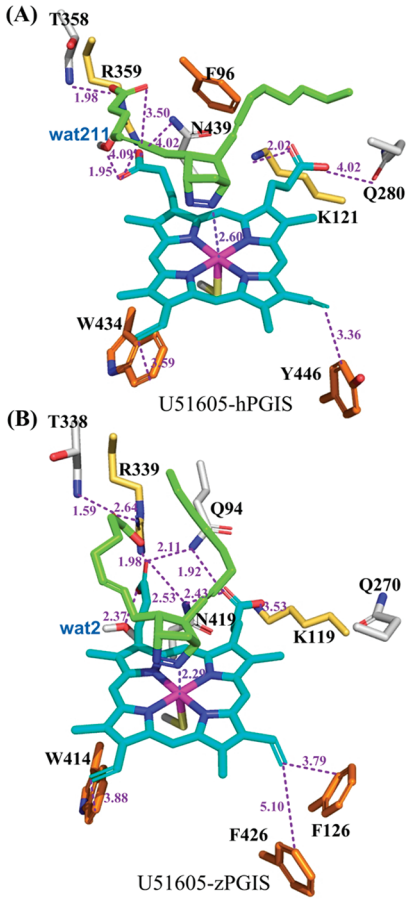

Figure 6. Molecular structure analyses for U51605-bound (A) hPGIS and (B) zPGIS complexes. The active site structural changes associated with binding of the substrate analogue, in which U51605 and heme are represented as green and light blue sticks, respectively, with nitrogen atoms in blue and oxygen in red, are shown. The protein residues encompassing the heme peripheral group and the binding of U51605 with its long side chain, resulting in a new hydrogen network, are also indicated.

C-11 nitrogen of U51605 is coordinated to the heme iron at a distance of 2.60 Å, and the C-9 nitrogen is slightly farther away from iron with a distance of 3.03 Å and is hydrogen-bonded to the side chain amide nitrogen of N287 at a distance of 2.80 Å (also in Table 3). Most water molecules in the propionate regions are extruded from U51605 binding. New hydrogen bonds are formed between the α-chain carboxylate group of U51605 and residues T358 and R359. Furthermore, the 7-propionate group is slightly pushed down toward the pyrrole ring, as assessed by the decrease of the inversion angle χ (see Figure 2 for details) from 26° to 19° (Table 4). As a result, 7-propionate forms a salt bridge and hydrogen bond with R359 and N439, respectively. Nonetheless, the 6-propionate is pushed downward to the proximal side of the heme, as evidenced by the change of χ from +56° to −7°, forming a weak hydrogen bond and a salt bridge with Q280 and K121, respectively. This projection clearly indicates that the binding of the substrate analogue with its long side chain disrupts the water cluster−propionate hydrogen-bonding network, thereafter establishing a new hydrogen network around the heme moiety in hPGIS. Similar water extrusion upon U51605 binding was also observed for zPGIS, comparing Figure 5B with Figure 6B. The water exclusion results in rearrangements of the hydrogen-bonding network, so that 7-propionate interacts directly with R339, N419, and Q94, while 6-propionate reacts with K119 and Q94 (Figure 6B).

Whereas the bending vibration is susceptible to the heme−protein interactions, the stretching vibration is sensitive to the degree of electronic conjugation and hence is dependent on the vinyl torsion $\tau(C_\alpha C_\beta C_a C_b)$ angle that alters the degree of π-bonding strength. To better analyze a possible change of the vinyl orientation upon ligand binding, both X-ray crystallography[11] and MD simulation were employed to compare the differences in torsion angles between resting and ligand-bound PGIS. The torsion angle ($\tau(C_\alpha C_\beta C_a C_b)$ defined in Figure 2) shows different modes of motion for the 2- and 4-vinyl groups (Table 4). MD simulations suggest that, in the resting hPGIS, the vinyls are partially flexible to rotate. The 4-vinyl rotates with a torsion angle between 153° and 66°, whereas the 2-vinyl rotates with τ between −150° and −137°. The vinyl rotations are mainly hindered by the adjacent methyl groups and amino residues of W434 and Y446 in hPGIS (W414 and F126 in zPGIS). Introduction of U51605 into the heme pocket induces the porphyrin plane to be more flattened as compared to the ligand-free structure, whereas the peripheral vinyl groups face more steric hindrance against amino acid residues, thereby limiting rotational flexibility. As a result, the orientation of 2-vinyl is further

restricted (τ is between $-166°$ and $-150°$), whereas 4-vinyl retains similar flexibility with τ between 147° and 74°. The torsion angle of the vinyls from the crystallographic data[11] gives values for 2- and 4-vinyl in the resting zPGIS of $-162°$ and 160°, and values of 178° and $-140°$, respectively, for the U51605-bound zPGIS. In brief, the vinyl torsion analysis for both hPGIS and zPGIS suggests that substrate binding should lead the 2-vinyl orientation to be more restricted to the heme macrocycle plane than 4-vinyl with respect to out-of-plane motion.

DISCUSSION

The lack of a crystal structure for substrate analogue-bound hPGIS and a poorly defined position of heme propionate in the resting hPGIS structure have hampered the elucidation of the structure/function relationship at the active site. With RR spectra and MD modeling provided in this study, a clear picture can be drawn to unveil the interactions among amino acid residues, heme, and substrate, particularly from the study of low-frequency RR signals that are sensitive to the structural changes in the propionate and vinyl groups.

Spin and Coordination States of the Resting and Ligand-Bound hPGIS and zPGIS. Table 1 lists the porphyrin skeletal stretching frequencies (1300−1700 cm^{-1}) of resting hPGIS and zPGIS which unequivocally demonstrated that the resting enzymes are six-coordinate, low-spin ferric heme species with thiolate and water as the axial ligands. The assignment of spin and coordination states is also in good agreement with our previous studies from MCD, EPR,[9] and the zPGIS crystal structure.[11] Notably, the current study is in contrast with the resting hPGIS crystal structure where the sixth ligand (water molecule) is absent.[10] It should also be noted that it is not uncommon that a mammalian P450, such as P450 3A4,[35] is found to be six-coordinate in solution but five-coordinate in the crystal structure. We thus argue that a five-coordinate hPGIS structure is a crystallographic artifact. Addition of a substrate analogue (U46619, U51605, or U44069) or an inhibitor/ligand (minoxidil, clotrimazole, or miconazole) to hPGIS and zPGIS causes few changes in the high-frequency RR region, indicating a six-coordinate, low-spin ferric heme species for ligand-bound hPGIS and zPGIS. On the basis of optical difference spectra,[8] U44069 has long been thought to induce a five-coordinated complex of PGIS. Our data showed that, in U44069-bound hPGIS and zPGIS, the υ_4, υ_3, υ_2, and υ_{10} vibrations at 1374, 1502, 1582, and 1638 cm^{-1}, respectively, are characteristics of a six-coordinate, low-spin species. The RR result is consistent with our previous EPR work, indicating a low-spin heme in the U44069−hPGIS complex.[9] Also, we are able to show, from the low-frequency RR data and MD simulation, a possible structure of U44069-bound PGIS, albeit at less favorable free energy (vide infra). Notably, a similar discrepancy was found in TXAS studies in which U46619−TXAS was first thought to be a five-coordinate species from the absorption spectral study but was later challenged by RR study to be a six-coordinate, low-spin species.[13]

Effect of Ligand Binding on Propionate Modes and the Associated Changes of the Conformations. Despite high similarities in enzymatic activity and crystallographic structure between the resting hPGIS and zPGIS,[10,11] low-frequency RR spectra have revealed salient differences in propionate−protein matrix interactions. One strong propionate bending vibration is seen at 386 cm^{-1} in hPGIS, accompanied by a very minor shoulder at 370 cm^{-1} (Table 2), whereas zPGIS yields a very different ratio (97:3 in hPGIS as compared to 79:21 in zPGIS) of the two modes. This is interpreted from crystallographic and MD study as reflecting the distinct hydrogen-bonding networks in the propionate groups of hPGIS and zPGIS (Figure 5). Previous studies have reported that the heme propionate bending frequency in a given protein increases as the number of hydrogen bonds to the propionates increases.[13,36] Thus, two modes of 370 and 387 cm^{-1} in zPGIS could presumably be attributed to differences in the hydrogen-bonding environment between 6- and 7-propionates. The higher number and hence more constraint of hydrogen bonds in the 7-propionate is associated with a higher frequency, i.e., 387 cm^{-1}, as compared with that of 6-propionate, which interacts only with K119 at 370 cm^{-1}. In contrast, 6-propionate of hPGIS interacts not only with K121 but also with water molecules and Q280. Furthermore, the multiple H-bonds with naturally different directionality networking water molecules in the 7-propionate (Figure 5) could give rise to rapidly interchanging conformers that are responsible for the broad band of 387 cm^{-1}. Along the same line, the interchanging conformers in 6-propionate of hPGIS (Figure 5A) lead to the weaker shoulder at 370 cm^{-1}. This assignment is tentative, and further work such as specifically isotope labeled heme is needed to provide direct support for assignment of the propionate bending modes.

Binding of substrate analogues (U46619, U51605, or U44069) to hPGIS induces a shift of the propionate bending vibration to a lower frequency at ~381 cm^{-1}, indicating the perturbation and rearrangement of the hydrogen-bonding networks. Results from MD simulations, as illustrated in Figures 5 and 6, reveal that the binding of substrate analogue U51605 disrupts the propionate hydrogen-bonding network by expelling most water molecules, and in turn forming new hydrogen bonds (or salt bridges) with the protein matrix along with a hydrogen bond between the carboxylate group of the substrate analogue and 7-propionate of the heme. Concomitantly, 6-propionate is drastically pushed downward to the proximal side of the heme so that the substrate analogue can sit snugly at the active site. Similar structural changes were observed for zPGIS upon U51605 binding (Figures 5B and 6B), accompanied by RR spectral shift of the propionate bending mode from 387 and 370 cm^{-1} to 383 cm^{-1} and a shoulder peak around 370 cm^{-1}, respectively (Figure 4B, trace c). In contrast, only a single propionate mode at 380 cm^{-1} with a significant Lorentzian component and narrower bandwidth was seen in the zPGIS complexed with U46619 (trace b in Figure 4B and Table 2). This difference can be explained by arguing that a hydrogen bond is formed between 6-propionate and 15-OH of U46619 (Figure S3 in the Supporting Information), which is absent in U51605 (Figure 6B).

Notably, U44069, which also has the 15-OH group, exhibits RR spectral shifts resembling U51605 (Figure 4B, trace d). Our MD result, given in Figure S3 of the Supporting Information, shows that the C9−O of U44069 binds the heme iron, unlike C11−O binding from U46619, in such a manner that the ω chain of the analogue rises high on the distal side, making the 15-OH group unable to form a hydrogen bond with 6-propionate (Figure S3 in the Supporting Information). This U44069−PGIS complex, however, is less stable than the U46619-bound PGIS complex, as revealed by the theoretical calculations (binding energies of −64.25 and −79.31 kcal/mol for U44069- and U46619-bound PGIS, respectively) and experimental results (dissociation constants of >190 and 36 μM for U44069- and

U46619-bound PGIS, respectively), and is unlikely a bona fide configuration for PGIS catalysis.

In contrast to the distinct responses upon binding of substrate analogues, the spectral patterns associated with the propionate bending modes in both hPGIS and zPGIS show negligible change upon binding of minoxidil, clotrimazole, or miconazole, indicating that these inhibitors/ligands do not interact with the propionate groups and hence have few interactions with the hydrogen-bonding network. This result is consistent with the crystal structure of minoxidil-bound hPGIS, in which most water molecules are retained and the positions of propionate relative to the pyrrole rings are unaltered with respect to those of the resting hPGIS.[11] It should also be noted that such RR discrimination between substrate analogues and inhibitors is not observed for its counterpart enzyme TXAS,[13] which catalyzes an isomerization of PGH_2 to give rise to thromboxane A_2 along with a fragmentation reaction to 12-hydroxy-5,8,10-heptadecatrienoic acid and malondialdehyde at a molar ratio of 1:1:1.[8] As shown in Table 2, TXAS has RR shifts on binding of substrate analogues (U44069 and U46619) similar to those on binding of inhibitor miconazole. Taken together, these data suggest that PGIS confers substrate-specific conformational changes, at least partly, by reshuffling of hydrogen-bonding networks with the heme propionates so that PGH_2 sits snugly at the active site for isomerization toward PGI_2 as the only pathway. We thus postulate that PGH_2 may not be so securely bound at the TXAS active site and therefore has more space to exercise fragmentation besides isomerization reaction.

Comparative Studies of Vinyl Conformations of the Resting and Ligand-Bound hPGIS and zPGIS. The vinyl vibration mode is sensitive to the orientation of the heme vinyl groups.[12−14,28,33,34,38] A number of heme proteins have been reported to have two vinyl stretching vibrations ($\upsilon_{C=C}$) at about 1620 and 1630 cm^{-1}, implying that the two vinyl groups have different orientations.[14,28] The isotopic labeling experiments would conclusively define the corresponding spectral bands for the 2- and 4-vinyl groups.[12,33,37] Density functional theory calculations suggest that the higher frequency is assigned to the vinyl group with a larger torsion angle of the out-of-plane conformer and the lower frequency to the in-plane conformer.[28] Moreover, earlier studies have suggested that the ∼410 cm^{-1} vinyl bending mode is associated with an in-plane vinyl conformer with a stretching mode at 1620 cm^{-1}, while the bending mode with higher frequency corresponds to the out-of-plane vinyl conformer with a stretching mode around 1630 cm^{-1}.[13,14,37] As evidenced by crystallography[11] and our current MD simulation, substrate binding leads to the 2- and 4-vinyl orientations of PGIS adopting the in-plane and out-of-plane conformations, respectively. We thus tentatively assigned vinyl stretching bands around 1620 and 1630 cm^{-1} to be associated with the in-plane and out-of-plane motions of vinyls.

In a pioneering study by Marzocchi and Smulevich,[34] an empirical relationship between the vinyl orientations and the $\upsilon_{C=C}$ vinyl stretching wavenumbers has been established among peroxidases. In this study, we then made an attempt to plot the $\upsilon_{C=C}$ vinyl stretching wavenumbers versus the vinyl torsion $\tau(C_\alpha C_\beta C_a C_b)$ angle (Table 4) obtained from crystallography[11] and MD simulations of PGIS. Figure S5 (Supporting Information) shows the dependence of the vinyl orientations and the vinyl stretching frequencies. The results may help to rationalize the slight variation of the stretching bands at 1620 and 1630 cm^{-1} among the PGIS forms (see Figure S1 of the Supporting Information) in relation to the flexibility of 2- and 4-vinyls.

Evidently, our data reveal that the distinctive differences in protein-specific effects can be detected in the more pronounced RR signals for $\delta(C_\beta C_a C_b)$ vinyl bending than for ($\upsilon_{C=C}$) stretching. The low-frequency spectral patterns show more distinctive responses upon binding of substrate analogues. The resting enzyme of hPGIS/zPGIS shows two modes of 412 and 426 cm^{-1} (421 cm^{-1} in zPGIS), which change to ∼404 and 428 cm^{-1} upon the binding of substrate analogues (Table 2). Introducing inhibitor does not perturb much of the vinyl bending modes because the deconvolution data are similar to those of the resting state.

The above results unambiguously indicate that site-specific interactions occur in substrate-bound PGIS, which preferentially stabilize different vinyl torsional conformers for the 2- versus 4-vinyls. Together, the crystallographic analysis and MD study demonstrate that incorporating a substrate analogue into the heme pocket imposes more restriction for the two vinyl groups into an in-plane and out-of-plane conformation. The MD study suggests that when the substrate analogue sits snugly at the active site, 2-vinyl is supposed to adopt a more in-plane conformation via its interaction with W434 (W414 in zPGIS), thus increasing conjugation with the porphyrin ring π system (Figure 6). This conjugation might be responsible for the downshift of the 412 cm^{-1} mode to ∼404 cm^{-1}. Consistent with previous works, the vinyl substituents in protoheme are in a different conjugated disposition with respect to the porphyrin ring, therefore resulting in a significant influence on the RR spectra.[12−14,28,33,34,38]

Early studies on P450 BM3 have pointed out that steric interaction between the residue and the vinyl groups might be involved in regulation of the heme redox potential.[14,39] Substitution of the highly conserved F393 near the 2-vinyl group results in a significant change in the heme redox potential. It is thus plausible that W434 controls the reaction by changing the redox potential of PGIS upon PGH_2 binding. It is thus intriguing to speculate that W434 may play a role in hPGIS catalysis. Additionally, we have proposed in our previous high-field EPR study residue Y446, which interacts with 4-vinyl, as the plausible residue to form a tyrosyl radical in the reaction of PGIS with peroxide.[40]

■ CONCLUSION

The RR spectra and MD simulations performed in this study, together with previous X-ray determination for PGIS structures, provide a firm basis for the examination of the heme propionate and vinyl bending modes at the molecular level. Several points have emerged from the present study: (1) Despite the fact that the water molecules in the propionate region cause dissimilar microenvironments of the heme pocket in the resting states of hPGIS and zPGIS, the side chains of the substrate analogue induce a distinctive perturbation of the propionate bonding and expulsion of networking water molecules, resulting in a very similar interaction mode for both hPGIS and zPGIS. (2) The conformational changes in the heme and protein matrix are manifested by substrate analogue binding, in particular of U46619, but not by inhibitor/ligand (minoxidil, clotrimazole, or miconazole) binding. (3) The binding of a substrate analogue rearranges the heme environment, which in turn forces the 2-vinyl group to adopt a more restricted in-plane conformation.

We thus propose that a similar mechanism is operative for the authentic substrate PGH_2, in which reshuffling of

hydrogen-bonding networks with the propionates and a more planar vinylheme structure are a prerequisite conformation prior to the enzymatic reaction. Our results also reveal that substrate analogue-induced RR shifts are drastically different from inhibitor-induced RR shifts, a phenomenon that is not observed for TXAS. From a mechanistic viewpoint, PGIS represents a ligand-specific heme conformation change to accommodate the substrate binding. Such a substrate-induced modulation of the heme conformation leads to the isomerization of PGH_2 with high product fidelity to PGI_2 by PGIS.

■ ASSOCIATED CONTENT

Supporting Information. Simulation and characterization details. This material is available free of charge via the Internet at http://pubs.acs.org.

■ AUTHOR INFORMATION

Corresponding Author
034407@mail.fju.edu.tw; hcyang_chem@mail.fju.edu.tw; chop@ntu.edu.tw

■ ACKNOWLEDGMENT

We thank Dr. Ah-Lim Tsai for his valuable comments and Li-Ru Lin for her technical assistance. This work was supported by Grant NSC 99-2113-M-030-004-MY2 from the National Science Council of the Republic of China and Grant 1095310-40982-2 from Fu-Jen Catholic University. We also thank the National Center for High-Performance Computing for computational resources.

■ REFERENCES

(1) Vane, J. R.; Botting, R. M. *Am. J. Cardiol.* **1995**, *75*, 3A–10A.
(2) Geraci, M. W.; Gao, B.; Shepherd, D. C.; Moore, M. D.; Westcott, J. Y.; Fagan, K. A.; Alger, L. A.; Tuder, R. M.; Voelkel, N. F. *J. Clin. Invest.* **1999**, *103*, 1509–15.
(3) Iwai, N.; Katsuya, T.; Ishikawa, K.; Mannami, T.; Ogata, J.; Higaki, J.; Ogihara, T.; Tanabe, T.; Baba, S. *Circulation* **1999**, *100*, 2231–6.
(4) Moncada, S.; Gryglewski, R.; Bunting, S.; Vane, J. R. *Nature* **1976**, *263*, 663–5.
(5) DeWitt, D. L.; Smith, W. L. *J. Biol. Chem.* **1983**, *258*, 3285–93.
(6) Ullrich, V.; Castle, L.; Weber, P. *Biochem. Pharmacol.* **1981**, *30*, 2033–6.
(7) Hara, S.; Miyata, A.; Yokoyama, C.; Inoue, H.; Brugger, R.; Lottspeich, F.; Ullrich, V.; Tanabe, T. *J. Biol. Chem.* **1994**, *269*, 19897–903.
(8) Hecker, M.; Ullrich, V. *J. Biol. Chem.* **1989**, *264*, 141–50.
(9) Yeh, H. C.; Hsu, P. Y.; Wang, J. S.; Tsai, A. L.; Wang, L. H. *Biochim. Biophys. Acta* **2005**, *1738*, 121–32.
(10) Chiang, C. W.; Yeh, H. C.; Wang, L. H.; Chan, N. L. *J. Mol. Biol.* **2006**, *364*, 266–74.
(11) Li, Y. C.; Chiang, C. W.; Yeh, H. C.; Hsu, P. Y.; Whitby, F. G.; Wang, L. H.; Chan, N. L. *J. Biol. Chem.* **2008**, *283*, 2917–26.
(12) Podstawka, E.; Mak, P. J.; Kincaid, J. R.; Proniewicz, L. M. *Biopolymers* **2006**, *83*, 455–66.
(13) Chen, Z.; Wang, L. H.; Schelvis, J. P. *Biochemistry* **2003**, *42*, 2542–51.
(14) Chen, Z.; Ost, T. W. B.; Schelvis, J. P. M. *Biochemistry* **2004**, *43*, 1798–808.
(15) Kincaid, J. R. *Resonance Raman Spectra of Heme Proteins and Model Compounds*; Academic Press: New York, 2000; Vol. 7, pp 225−91.
(16) Spiro, T. G. *Adv. Protein Chem.* **1985**, *37*, 111–59.
(17) Tosha, T.; Kagawa, N.; Ohta, T.; Yoshioka, S.; Waterman, M. R.; Kitagawa, T. *Biochemistry* **2006**, *45*, 5631–40.
(18) Mak, P. J.; Kaluka, D.; Manyumwa, M. E.; Zhang, H.; Deng, T.; Kincaid, J. R. *Biopolymers* **2008**, *89*, 1045–53.
(19) Zou, M.; Jendral, M.; Ullrich, V. *Br. J. Pharmacol.* **1999**, *126*, 1283–92.
(20) Hecker, M.; Ullrich, V. *Biochem. Pharmacol.* **1988**, *37*, 3363–65.
(21) Steinhilber, D.; Jaschonek, K.; Knospe, J.; Morof, O.; Roth, H. J. *Arzneimittelforschung* **1990**, *40*, 1260–3.
(22) Rappe, A. K.; Casewit, C. J.; Colwell, K. S.; Goddard, W. A.; Skiff, W. M. *J. Am. Chem. Soc.* **1992**, *114*, 10024–35.
(23) Casewit, C. J.; Colwell, K. S.; Rappe, A. K. *J. Am. Chem. Soc.* **1992**, *114*, 10035–46.
(24) Brooks, B. R.; Bruccoleri, R. E.; Olafson, B. D.; States, D. J.; Swaminathan, S.; Karplus, M. *J. Comput. Chem.* **1983**, *4*, 187–217.
(25) Abe, M.; Kitagawa, T.; Kyogoku, Y. *J. Chem. Phys.* **1978**, *69*, 4526–34.
(26) Choi, S.; Spiro, T. G. *J. Am. Chem. Soc.* **1983**, *105*, 3683–92.
(27) Li, X. Y.; Czernuszewicz, R. S.; Kincaid, J. R.; Su, Y. O.; Spiro, T. G. *J. Phys. Chem.* **1990**, *94*, 31–47.
(28) Kalsbeck, W. A.; Ghosh, A.; Pandey, R. K.; Smith, K. M.; Bocian, D. F. *J. Am. Chem. Soc.* **1995**, *117*, 10959–68.
(29) Wells, A. V.; Li, P.; Champion, P. M.; Martinis, S. A.; Sligar, S. G. *Biochemistry* **1992**, *31*, 4384–93.
(30) Schelvis, J. P.; Berka, V.; Babcock, G. T.; Tsai, A. L. *Biochemistry* **2002**, *41*, 5695–701.
(31) Mak, P. J.; Denisov, I. G.; Grinkova, Y. V.; Sligar, S. G.; Kincaid, J. R. *J. Am. Chem. Soc.* **2011**, *133*, 1357–66.
(32) Wang, J. S. Unpublished data.
(33) Hu, S.; Smith, K. M.; Spiro, T. G. *J. Am. Chem. Soc.* **1996**, *118*, 12638–46.
(34) Marzocchi, M. P.; Smulevich, G. *J. Raman Spectrosc.* **2003**, *34*, 725–36.
(35) Williams, P. A.; Cosme, J.; Vinkovic, D. M.; Ward, A.; Angove, H. C.; Day, P. J.; Vonrhein, C.; Tickle, I. J.; Jhoti, H. *Science* **2004**, *305*, 683–6.
(36) Peterson, E. S.; Friedman, J. M.; Chien, E. Y.; Sligar, S. G. *Biochemistry* **1998**, *37*, 12301–19.
(37) Smulevich, G.; Hu, S.; Rodgers, K. R.; Goodin, D. B.; Smith, K. M.; Spiro, T. G. *Biospectroscopy* **1996**, *2*, 365–76.
(38) Smulevich, G.; Feis, A.; Howes, B. D. *Acc. Chem. Res.* **2005**, *38*, 433–40.
(39) Ost, T. W.; Miles, C. S.; Munro, A. W.; Murdoch, J.; Reid, G. A.; Chapman, S. K. *Biochemistry* **2001**, *40*, 13421–9.
(40) Yeh, H. C.; Gerfen, G. J.; Wang, J. S.; Tsai, A. L.; Wang, L. H. *Biochemistry* **2009**, *48*, 917–28.